Energy Materials

Supplementary Materials

Sea urchin-like La-doped MnO_2 for electrocatalytic oxidation degradation of sulfonamide in water

Xia Wu[1,#], Ming Chen[2,#], Shuang Li[3,#], Xiaohan Liu[4], Xiaoxiang Xu[3,*], Weilong Wang[3], Wei Zhang[4,*], Rui Cao[4,*]

[1]Department of Otorhinolaryngology Union Hospital, Tongji Medical College, Huazhong University of Science and Technology, Wuhan 430022, Hubei, China.
[2]Department of Pediatrics Xiangyang Central Hospital, Affiliated Hospital of Hubei University of Arts and Science Xiangyang, Xiangyang 441021, Hubei, China.
[3]Department of Otorhinolaryngology-Head and Neck Surgery Zhongnan Hospital of Wuhan University, Wuhan 430071, Hubei, China.
[4]School of Chemistry and Chemical Engineering, Shaanxi Normal University, Xi'an 710119, Shannxi, China.
[#]Authors contributed equally.

[*]**Correspondence to:** Dr. Xiaoxiang Xu, Department of Otorhinolaryngology-Head and Neck Surgery, Zhongnan Hospital of Wuhan University, Wuhan 430071, Hubei, China. E-mail: zn003504@whu.edu.cn; Prof. Wei Zhang and Prof. Rui Cao, School of Chemistry and Chemical Engineering, Shaanxi Normal University, Xi'an 710119, Shannxi, China. E-mail: zw@snnu.edu.cn; ruicao@snnu.edu.cn

Calculation methods

The formula for the calculation of the Turnover Frequency (TOF) is as follows:

$$\mathrm{TOF} = \frac{j \times \mathrm{N_A}}{\mathrm{Z} \times \mathrm{F} \times \mathrm{n}} \quad (1)$$

$$\mathrm{n} = \mathrm{m} \times \mathrm{N} \quad (2)$$

j (mA/cm^2) denotes the current density measured at an overpotential of 470 mV; $\mathrm{N_A}$ denotes Avogadro constant; F denotes Faraday constant; Z denotes the number of electrons required to generate one product molecule; n denotes the surface concentration or exact number of active sites in the catalytic reaction. In OER, the n value is 4, representing the number of electrons transferred when one molecule of O_2 is formed. In Equation (2), m (g/cm^2) and N (g^{-1}) represent the load mass per square centimeter of electrode surface and the number of active sites per gram of catalyst, respectively.

The relationship between ECSA (cm^2) and C_{dl} (μF) is shown in Equation (3):

$$\mathrm{ECSA} = C_{dl}/C_s \quad (3)$$

The routes of electrocatalytic degradation of SA:

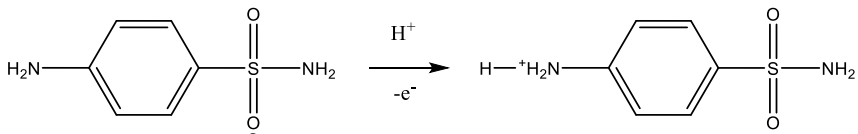

(4)

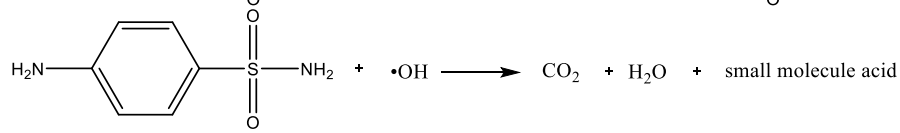

(5)

The formula for calculating the sulfonamide degradation rate:

$$\eta = \frac{\mathrm{C_0 - C_t}}{\mathrm{C_0}} \quad (6)$$

C_0 and C_t are the initial sulfonamide concentration and the concentration at time t, respectively.

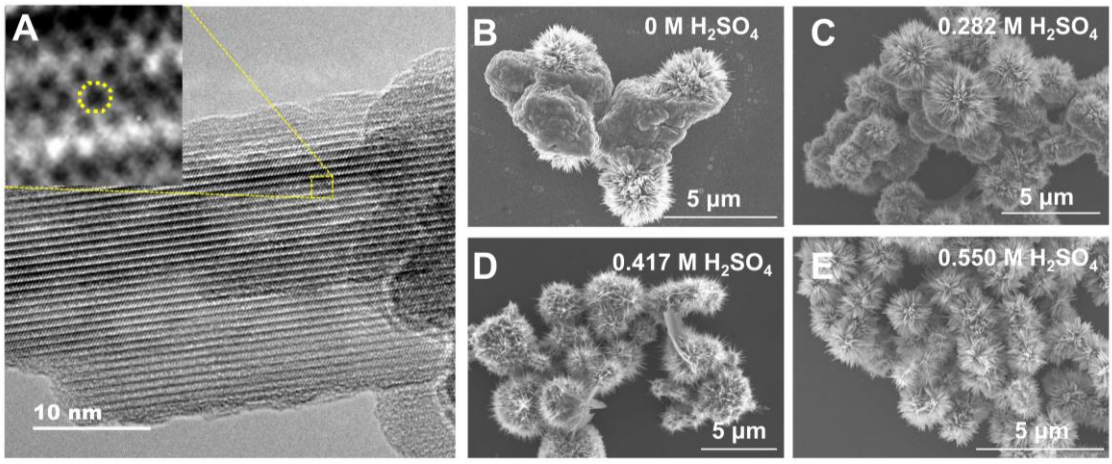

Supplementary Figure 1. (A) The HR-TEM image of α-MnO_2 (The inset shows the pore structure). The SEM images of MnO_2 synthesized with (B) 0 M, (C) 0.282 M, (D) 0.417 M, and (E) 0.550 M H_2SO_4.

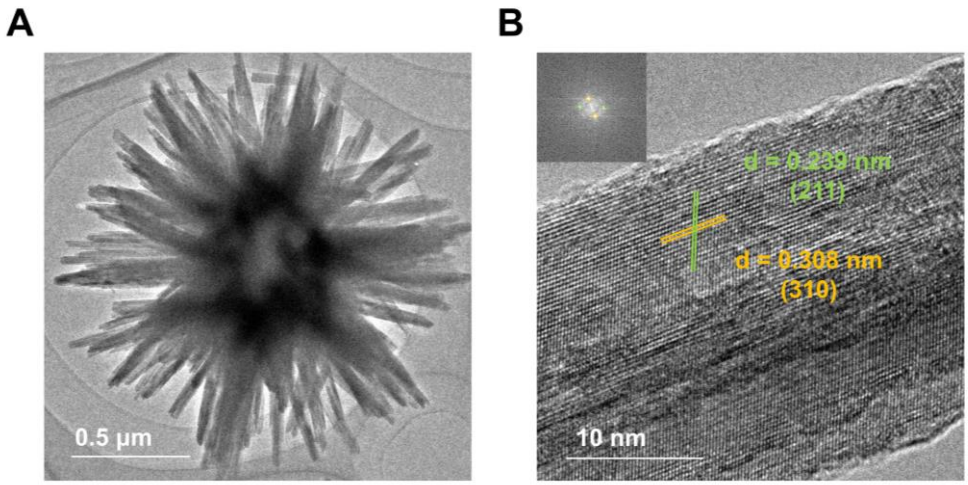

Supplementary Figure 2. (A) The TEM and (B) HR-TEM images of MnO_2 (The inset shows the corresponding FFT pattern).

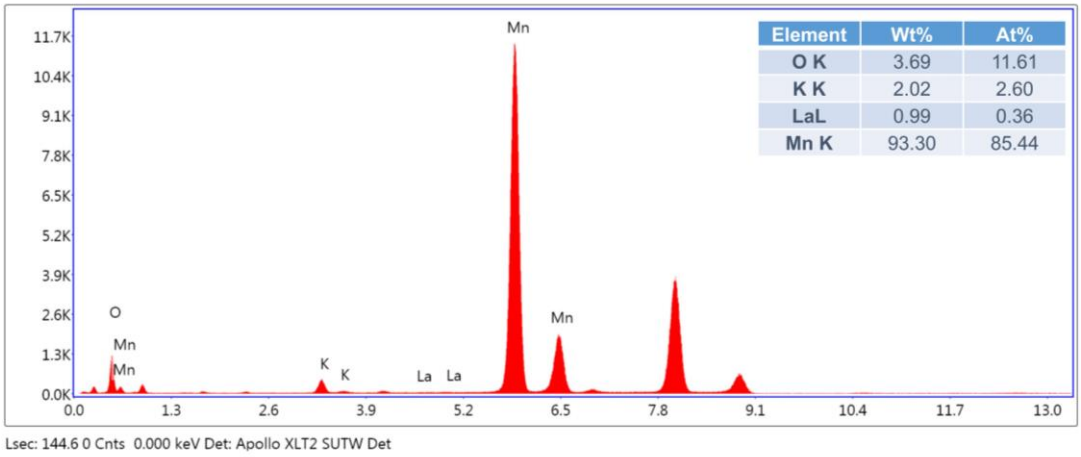

Supplementary Figure 3. The EDX spectrum of La-doped MnO_2.

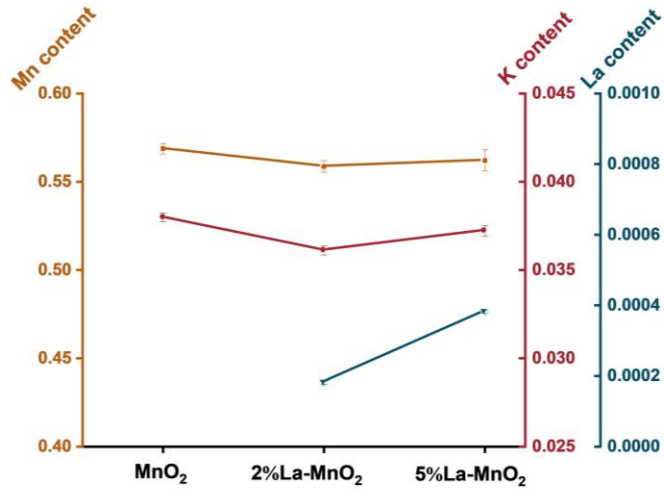

Supplementary Figure 4. The ICP-OES results for MnO_2, 2% La-doped MnO_2, and 5% La-doped MnO_2.

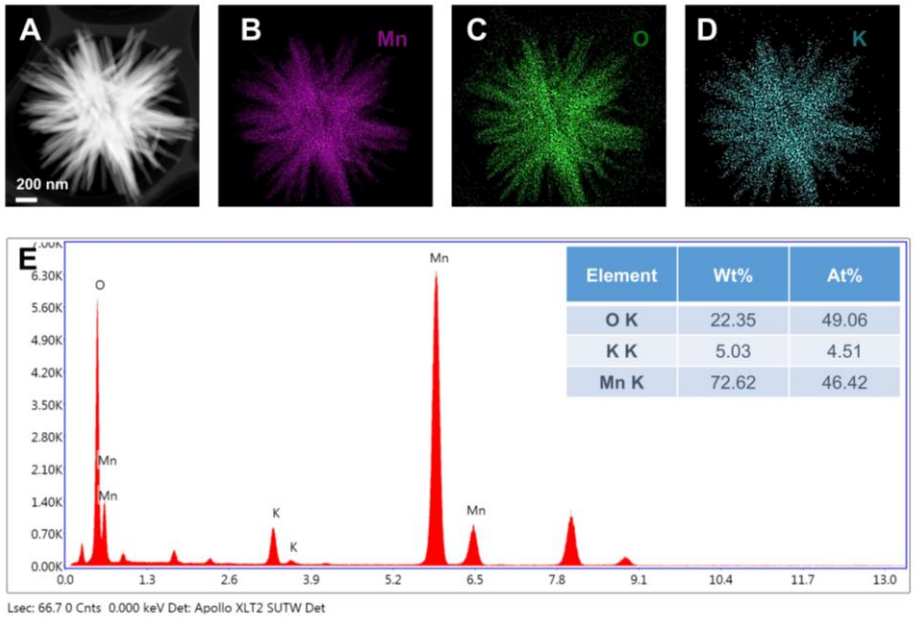

Supplementary Figure 5. (A-D) The HAADF-STEM image and the corresponding elemental mapping images of the MnO_2. (E) The EDX spectrum of pure MnO_2.

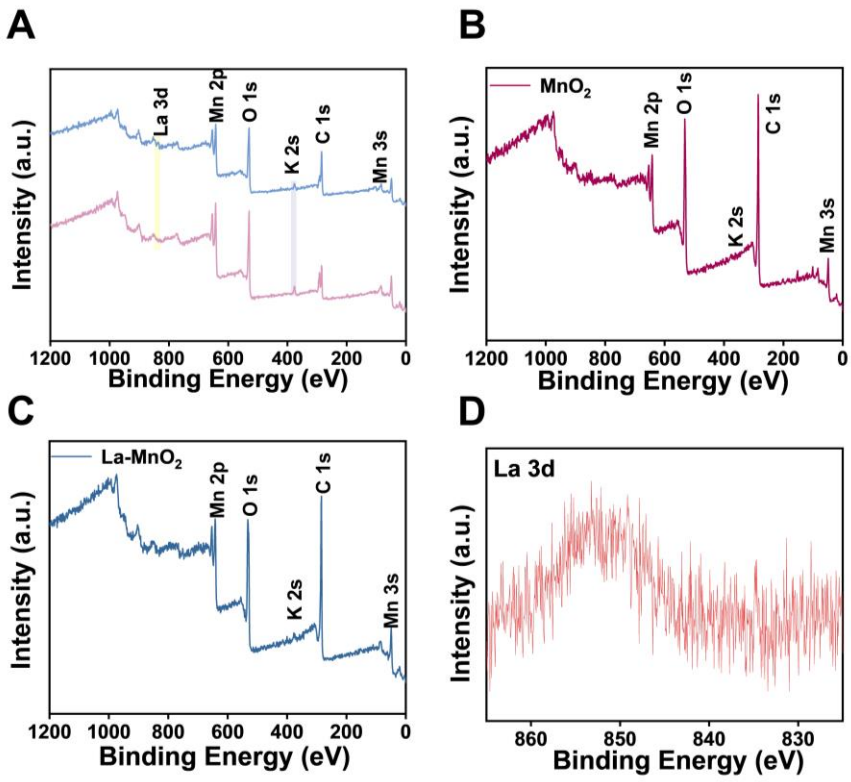

Supplementary Figure 6. (A) The XPS survey spectra of La-doped MnO_2 (top) and MnO_2 (bottom). The XPS survey spectra of (B) MnO_2 and (C) La-doped MnO_2 after OER. (D) The La 3d XPS spectrum of La-doped MnO_2 after OER.

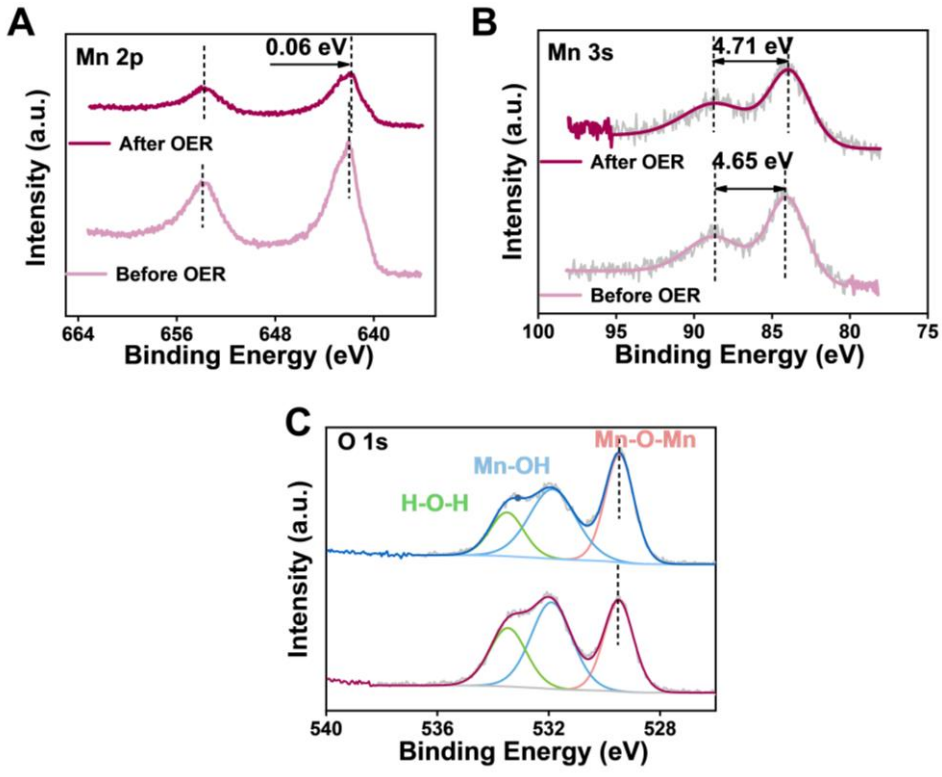

Supplementary Figure 7. (A) Mn 2p and (B) Mn 3s XPS spectra for MnO_2 before and after OER. (C) O 1s XPS spectra of La-doped MnO_2 (top) and MnO_2 (bottom).

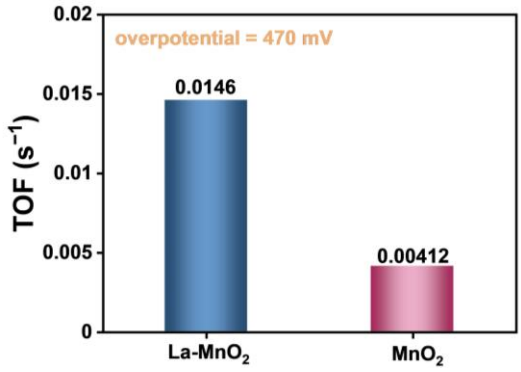

Supplementary Figure 8. The TOF for OER of La-doped MnO_2 and MnO_2 at an overpotential of 470 mV.

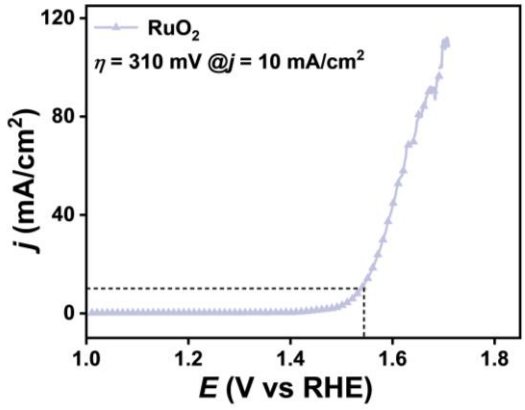

Supplementary Figure 9. The OER LSV polarization curve of RuO_2 in 1.0 M KOH.

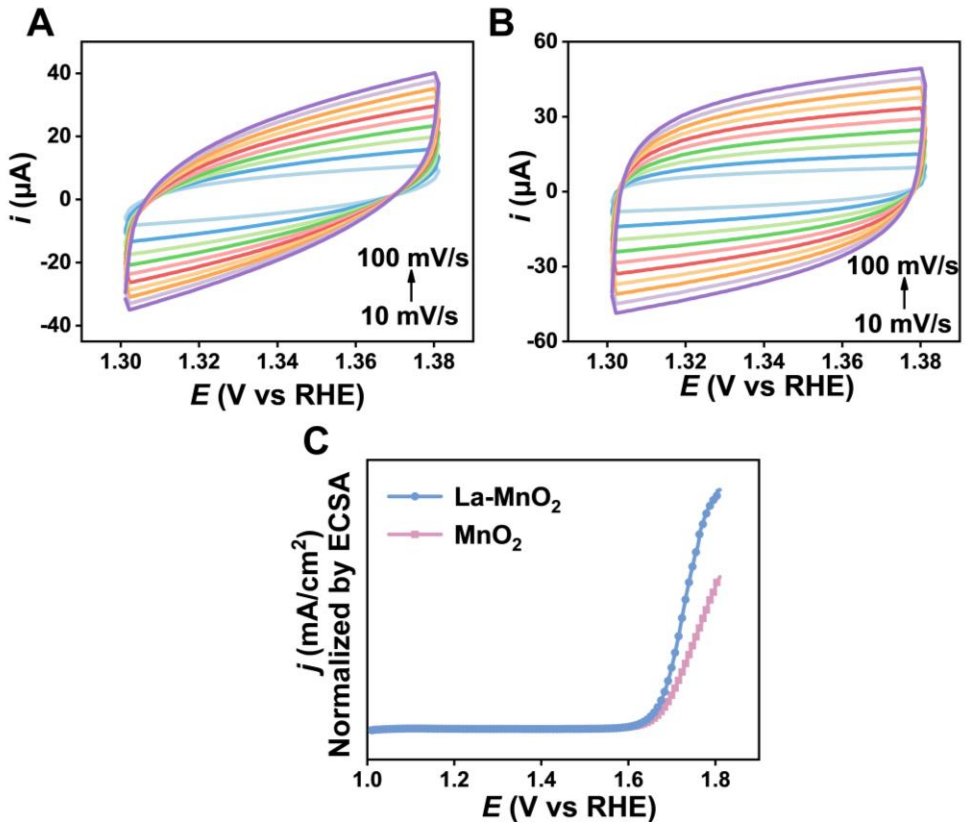

Supplementary Figure 10. The charging currents of (A) MnO_2 and (B) La-doped MnO_2 samples recorded in the non-Faradaic potential region at different scan rates. (C) The normalized OER activity of the two samples.

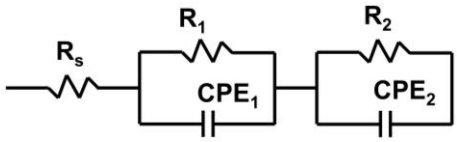

	R_s	R_1 (Ω)	CPE_1 (mF)	R_2 (Ω)	CPE_2 (mF)
MnO_2	6.642	31.71	746.3	203.7	787.4
La-MnO_2	5.834	19.63	475.9	126.2	776.4

Supplementary Figure 11. The equivalent circuit model (top) and the the fitted results for the two catalysts (bottom).

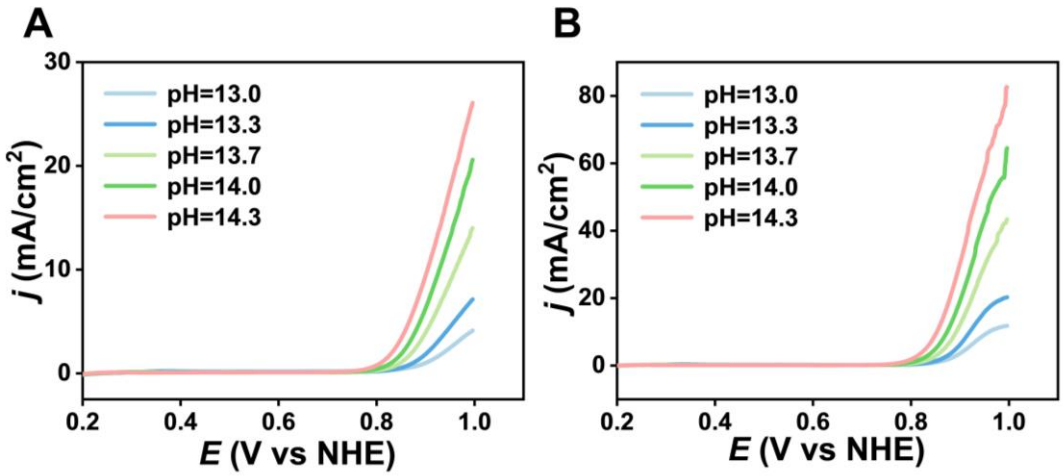

Supplementary Figure 12. The pH-dependent LSVs of (A) MnO_2 and (B) La-doped MnO_2 at a scan rate of 5 mV s^{-1}.

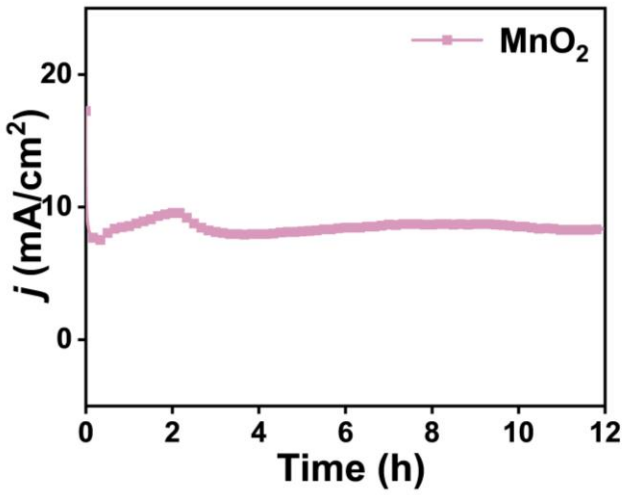

Supplementary Figure 13. The CPE of MnO_2 for OER at 1.75 V (*vs* RHE) without iR compensation.

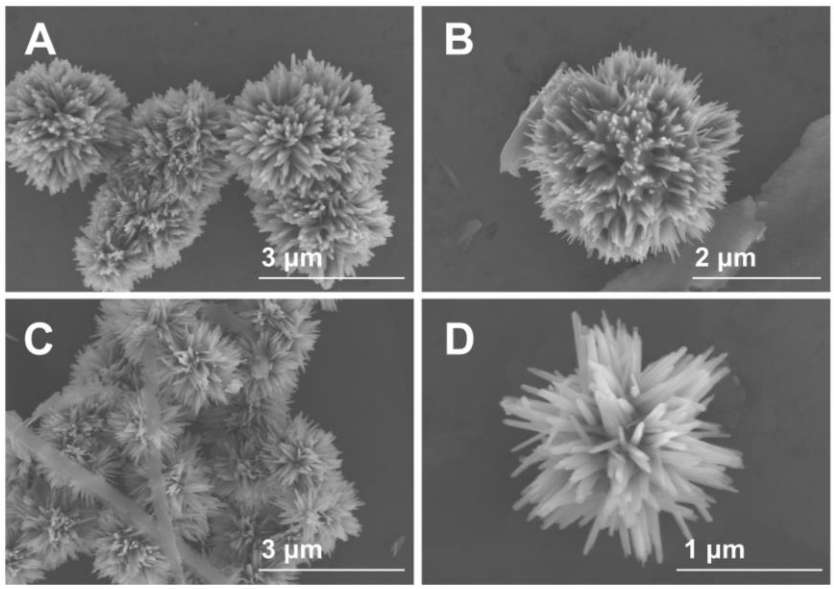

Supplementary Figure 14. The SEM images of (A, B) La-doped MnO_2 and (C, D) MnO_2 after CPE.

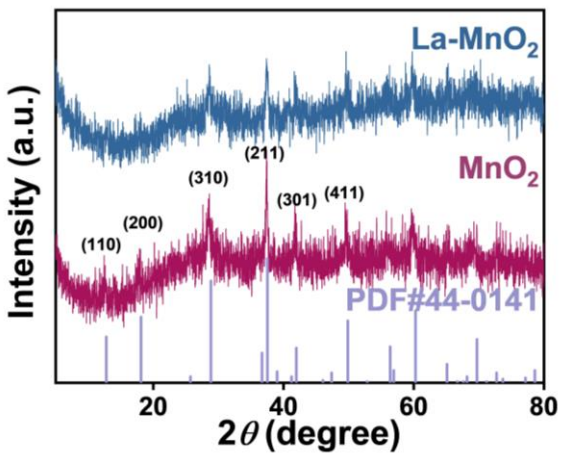

Supplementary Figure 15. The XRD patterns of La-doped MnO_2 and MnO_2 after OER.

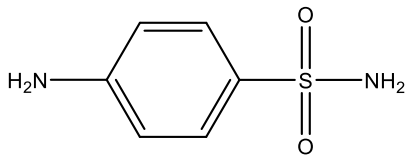

Supplementary Figure 16. The structure of SA.

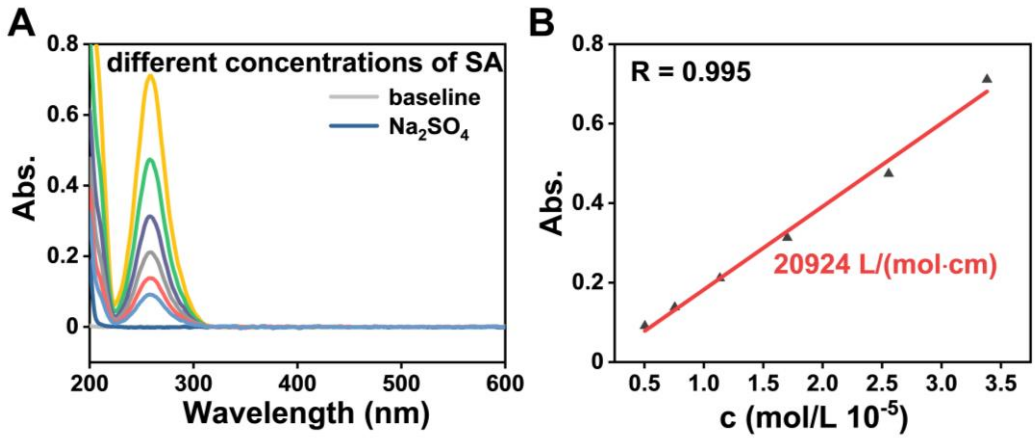

Supplementary Figure 17. (A) The UV-vis absorption spectra of solutions of Na_2SO_4 with different concentrations of SA. (B) The standard curve of SA in water.

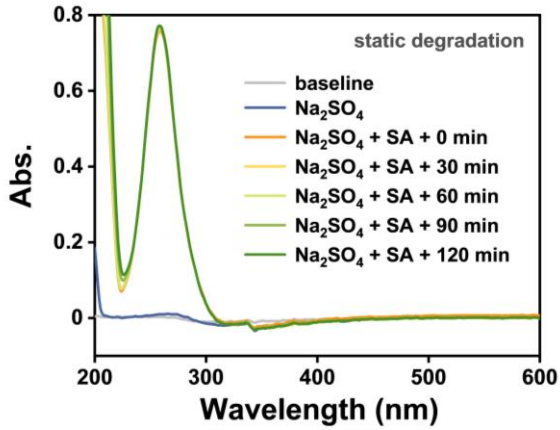

Supplementary Figure 18. The UV-vis absorption spectra of SA under static degradation.

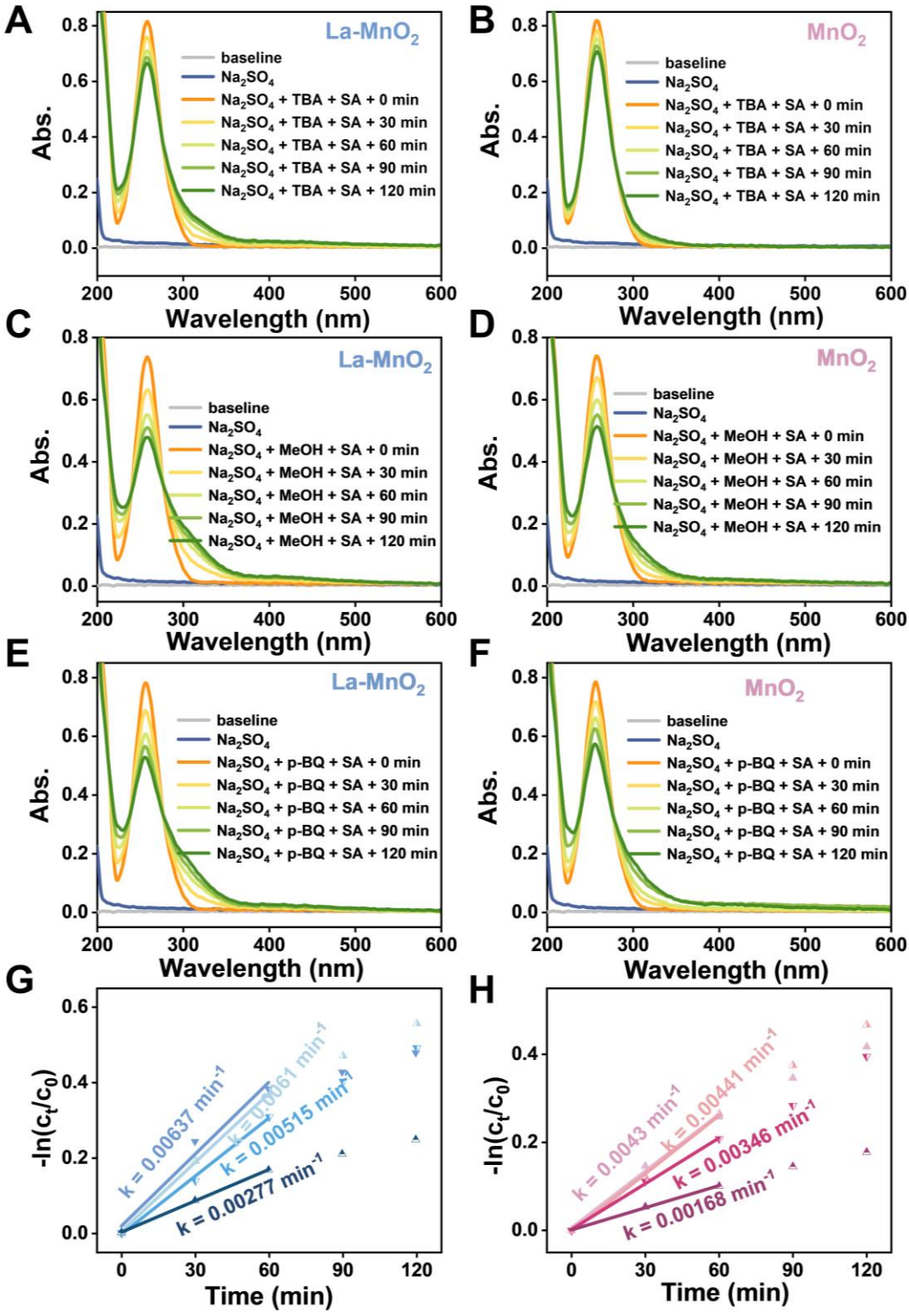

Supplementary Figure 19. The UV-vis absorption spectra of solutions containing Na_2SO_4 and SA, with the addition of (A, B) TBA, (C, D) MeOH, or (E, F) *p*-BQ during electrolysis for (A, C, and E) La-doped MnO_2 and (B, D, and F) MnO_2 catalysts at 2.1 V over various time intervals. The electrocatalytic degradation kinetics of SA with (G) La-doped MnO_2 and (H) MnO_2 catalysts in the presence of different radical scavengers.

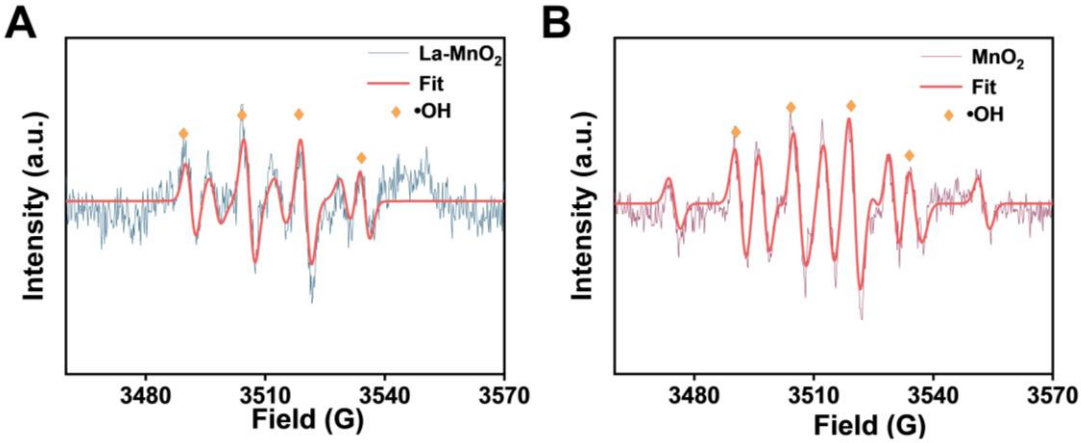

Supplementary Figure 20. EPR spectra of •OH in (A) La-doped MnO_2 and (B) MnO_2.

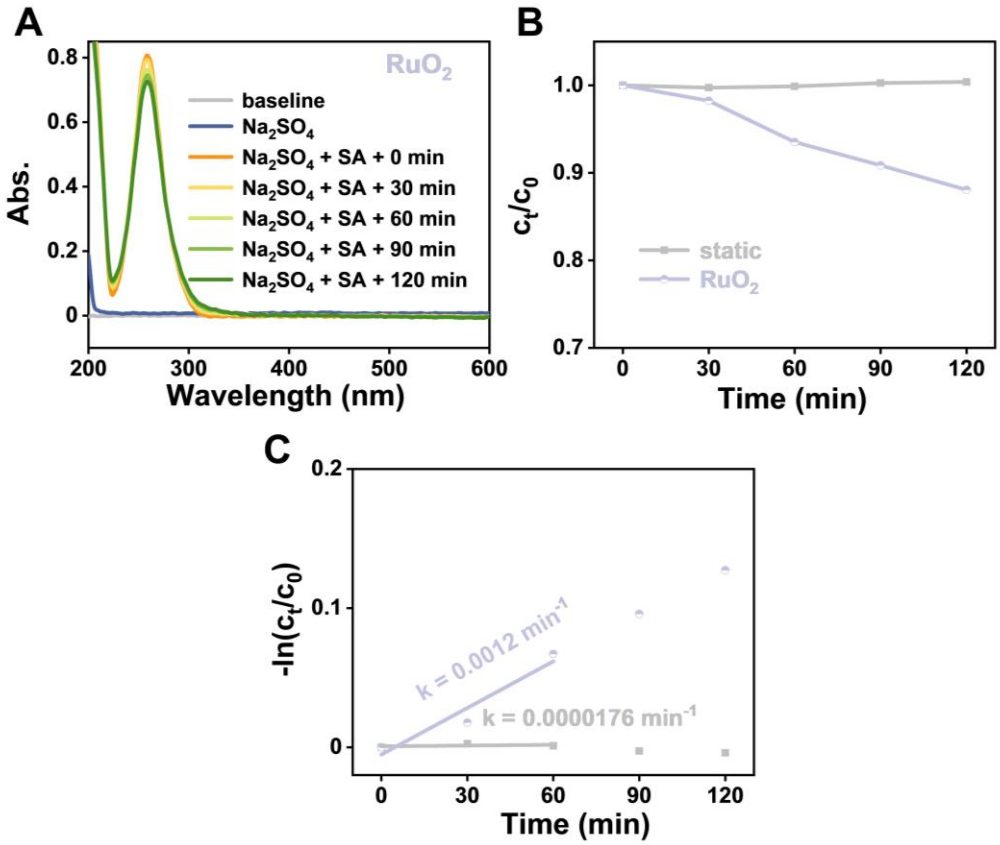

Supplementary Figure 21. (A) The UV-vis absorption spectra of a solution of Na_2SO_4 and SA during electrolysis by RuO_2 at 2.1 V for different times. (B) The comparison of the electrochemical degradation efficiency of RuO_2 and the static degradation efficiency. (C) The corresponding electrocatalytic degradation kinetics of SA.

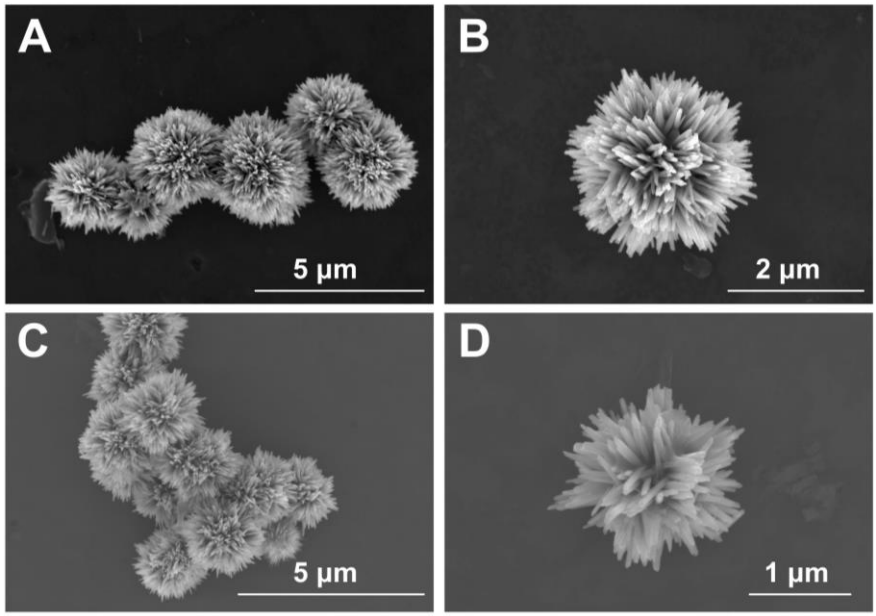

Supplementary Figure 22. The SEM images of (A, B) La-doped MnO_2 and (C, D) MnO_2 after SA degradation.

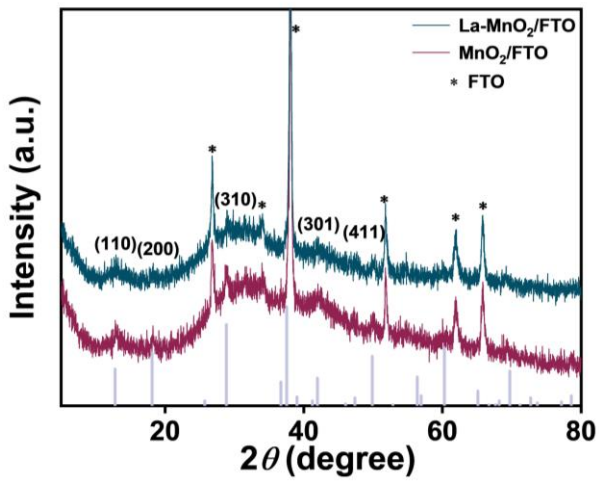

Supplementary Figure 23. The XRD patterns of La-doped MnO_2 and MnO_2 after SA degradation.

Supplementary Table 1. The La^{3+} ion leaching amount after 12 hours of constant potential electrolysis

Time (h)	12
La Concentration (ppb)	0.8436 ± 0.05

Supplementary Table 2. Comparison of OER performance of sea urchin-like α-MnO_2 catalyst with other recently reported Mn oxide electrocatalysts

Catalysts	Electrolyte	Overpotential (mV) @ 10 mA/cm^2	Tafel Slope (mV/dec)	Ref.
Sea urchin-like La-MnO_2	**1 M KOH**	**450**	**71**	**This work**
β-MnO_2	1 M KOH	561	187	[1]
τ-MnO_2	1 M KOH	527	188	[1]
Mn_3O_4	1 M KOH	890	343	[2]
α-MnO_2-NWN	1 M KOH	467	65.6	[3]
Mn_2O_3	1 M KOH	470 (@ 1 mA/cm^2)	-	[4]
2D Mn_3O_4	0.1 M KOH	670 (@ 5 mA/cm^2)	316	[5]
MnO_2@PFANI nanowire	1 M KOH	440	82	[6]
Mesoporous Mn_2O_3	0.1 M KOH	470	-	[7]
δ-MnO_2/CC	1 M KOH	495	179	[8]
MnO_2-$Ni_{0.002(M)}$	0.1 M KOH	445	86	[9]
Mo/α-MnO_2	1 M KOH	440	86	[10]
Al-doped Mn_3O_4	1 M KOH	450	109	[11]

REFERENCES

1. Qin, Y.; Liu, Y.; Zhang, Y.; et al. Ru-substituted MnO_2 for accelerated water oxidation: The feedback of strain-induced and polymorph-dependent structural changes to the catalytic activity and mechanism. *ACS Catal.* **2023**, *13*, 256-266. DOI: 10.1021/acscatal.2c04759
2. Wang, P.; Zhang, S.; Wang, Z.; et al. Manganese-based oxide electrocatalysts for the oxygen evolution reaction: A review. *J. Mater. Chem.* **2023**, *11*, 5476-5494. DOI: 10.1039/D2TA09039B
3. Chen, Y.; Yang, S.; Liu, H.; et al. An unusual network of α-MnO_2 nanowires with structure-induced hydrophilicity and conductivity for improved electrocatalysis. *Chinese J. Catal.* **2021**, *42*, 1724-1731. DOI: 10.1016/S1872-2067(21)63793-2
4. Wan, S.; Li, Y.; Xu, L.; et al. Autologous mn oxides as electrocatalysts to identify the origin of the water oxidation activity. *Mater. Today Sustain.* **2022**, *17*, 100106. DOI: 10.1016/j.mtsust.2021.100106
5. Chowde Gowda, C.; Mathur, A.; Parui, A.; et al. Understanding the electrocatalysis OER and ORR activity of ultrathin spinel Mn_3O_4. *J. Ind. Eng. Chem.* **2022**, *113*, 153-160. DOI: 10.1016/j.jiec.2022.05.024
6. Qin, L.; Zhang, W.; Cao, R. Hydrophilic MnO_2 nanowires coating with o-fluoroaniline for electrocatalytic water oxidation. *Chin. J. Struct. Chem.* **2023**, *42*, 100105. DOI: 10.1016/j.cjsc.2023.100105
7. Sa, Y. J.; Kim, S.; Lee, Y.; et al. Mesoporous manganese oxides with high-valent Mn species and disordered local structures for efficient oxygen electrocatalysis. *ACS Appl. Mater. Interfaces* **2023**, *15*, 31393-31402. DOI: 10.1021/acsami.3c03358
8. Liu, Y.; Ma, S.; Zhang, S.; et al. Enhanced water oxidation stability and activity in MnO_2 nanosheet arrays through Ti doping. *Fuel* **2024**, *374*, 132424. DOI: 10.1016/j.fuel.2024.132424
9. Bera, K.; Karmakar, A.; Karthick, K.; et al. Enhancement of the OER kinetics of the less-explored α-MnO_2 via nickel doping approaches in alkaline medium. *Inorg. Chem.* **2021**, *60*, 19429-19439. DOI: 10.1021/acs.inorgchem.1c03236
10. Chen, Y.; Yang, S.; Wang, T.; et al. Mo-doped α-MnO_2 for enhanced electrocatalytic water oxidation. *ChemSusChem* **2025**, *18*, e202401553. DOI: 10.1002/cssc.202401553
11. Liu, X.; Yang, S.; Li, S.; et al. The doping of Al^{3+} at the tetrahedral site of spinel

Mn_3O_4 for electrocatalytic water oxidation. *Chem. Eur. J.* **2025**, *31*, e202403720. DOI: 10.1002/chem.202403720